RESPONSE OF THE SMALL ICE DETECTOR (SID-2) TO ICE AND WATER CLOUD PARTICLES AND TO AEROSOLS, OBTAINED DURING FLIGHTS OF THE UK MET OFFICE/BAE-146 ATMOSPHERIC RESEARCH AIRCRAFT.

R. J. Cotton[1], Z. Ulanowski[2], E. Hirst[2], P. H. Kaye[2], R. S. Greenaway[2]
1. Met Office, Exeter, UK, richard.cotton@metoffice.gov.uk
2. Science and Technology Research Centre, University of Hertfordshire, Hatfield, UK

ABSTRACT

The Small Ice Detector 2 (SID-2) built by the University of Hertfordshire has been operated by the UK Met Office on the BAe-146 research aircraft during a large number of flights. These flights included runs in Stratocumulus, Cirrus, and mixed phase clouds, clear-sky flights over the sea and over desert surfaces. SID-2 is a laser scattering device which fits into a standard PMS canister to provide in situ data on cloud particle concentration, size and some information on the particle shape. The response of SID-2 to water drops, ice particles and aerosols are presented. Results include the particle size range and concentration capability, the discrimination of liquid and ice phase, and background problems.

1. INTRODUCTION

The in-situ measurement of cloud particle number concentration, size and (liquid/ice) phase are important for the study of cloud microphysics and for radiative properties. Being able to measure these properties of small cloud particles (of the order of a few microns in size) should for example, enable the onset of ice nucleation to be determined in a mixed-phase cloud. The Small Ice Detector 2 (SID-2) was built by the University of Hertfordshire to discriminate between super-cooled liquid drops and small ice particles, and to estimate the size of the ice particles which are generally below the size capability of current cloud particle probes. The SID-2 therefore complements the current ice particle probes (2D-C and CPI). While it is not designed to replace the FSSP for warm liquid drops in Sc, by comparison with the FSSP it can be validated.

2. SID-2 DESIGN AND OPERATION

SID-2 is an improved version of the first SID version, described in Hirst et. al. 2001. There are three important improvements: the probe inlet is open-path to reduce any possible shattering of large cloud particles, the spatial resolution of the photodetector is increased from 6 to 24 segments, and the data acquisition is capable of time-stamping individual particles.

The scattered light is detected by a hybrid photo-diode (HPD) which is a segmented silicon photodiode mounted in a vacuum tube with a photocathode. The HPD has 27 photodiode elements, with 3 central and 24 arranged azimuthally covering a forward scattering angle up to 20 degrees. The spatial scattering onto these outer elements give information about the particle shape. Spherical particles scatter light uniformly giving a uniform response across all 24 elements.

3. FLIGHT DATA

The flight data shown here was taken during a large number of flights which included runs in Stratocumulus, Cirrus, and mixed phase clouds, clear-sky flights over the sea and over desert surfaces. The details of the runs used are shown in Appendix C.

3.1 Behaviour in water only clouds: warm Stratocumulus and super-cooled wave cloud

Two flights are selected where aircraft instrumentation indicated that only liquid water was present: One was mainly in extensive Stratocumulus (flight B256) and the other in orographic lenticular cloud (flight B252) which was supercooled liquid water only.

The SID-2 response during one straight and level run in Stratocumulus is shown in fig. 1.

This was at 1600 ft above MSL with air temperature around 9°C. The SID-2 particle diameter measurement range covers the FFSSP range (which is from 2 to 47μm), so the concentration agreement is expected to be good if the sample volume has been estimated correctly. The SID-2 bulk-water content obtained from integration of the particle size spectrum is compared to the bulk-water probes. For all the runs, each at different altitude in the Stratocumulus, the agreement with the FSSP and bulk-water probes is good.

The cloud particle phase is determined by the scattering asymmetry factor, A_f, defined in Appendix B. A contour plot of frequency of occurance as a function of A_f and calculated particle size for this single run is shown in fig. 2. Most particles have $A_f < 8$, but there are significant numbers with larger A_f. Fig. 3 is a similar plot but for a run in a super-cooled liquid water wave cloud, where other aircraft instruments indicated no ice present. This was at FL250 with air temperature around -32°C. For this run, there are negligible numbers of particles with large A_f, confirming the no ice observation.

3.2 Behaviour in ice only clouds: frontal Cirrus

One flight in frontal Cirrus (B257) is selected. The SID-2 response during one straight and level run near the Cirrus top is shown in fig. 4. This was at FL320 with air temperature around -57°C. At this cold temperature, no liquid water will be present. Near the cloud top, all ice particles are small enough to be measured by the SID-2 without detector saturation. The SID-2 size distribution and calculated bulk-water content can be compared with that from the 2D-C. The number concentration for ice particles around the size overlap region is in good agreement. The under-reading of the Nevzorov total water content in ice cloud is expected. Fig. 5 shows that most particles have $A_f > 5$. This run with very small, more pristine ice particles, is a more difficult test for the SID-2 phase discrimination capability than using larger, possibly aggregated particles.

3.3 Behaviour in mixed-phase clouds: super-cooled Cumulus

One flight in Cumulus (B246) is selected. The SID-2 response during one straight and level runs near the Cumulus top is shown in fig. 6. This was at FL135 with air temperature around -9°C. The A_f values indicate that there are significant amounts of both liquid drops and ice particles present.

3.4 Behaviour in aerosols: industrial pollution and sea-salt

4. DISCUSSION

Data from the wave-cloud flight shows that the SID-2 detection limit for cloud particles (observed at the leading edge of the cloud) is around 3μm radius. This is due to the low laser power and photodetector dark current noise. The detector elements are saturated for cloud particles above 70μm radius (80μm radius for ice particles).

The SID-2 inlet design is open-path to reduce possible large particle shattering. As described in Field et. al. 2003, the distribution of particle inter-arrival times indicates where shattering is occurring.

Surrounding the small trigger volume is an extended sensing volume (60 times larger). The coincidence of particles in this sensing volume while another particle triggers the detector read-out will add to the scattered light intensity of the triggered particle. This will lead to a non-uniform azimuthal detector element response and lead to skewing the particle size distribution towards larger particle sizes. The probability of coincidence can be calculated using Poission statistics and depends on the particle concentration (there is a 5% probability when the concentration is 30cm^3). The coincidences might be displayed in the scattering patterns for the Stratocumulus run shown in fig. 7 typified by the particle 28.

There is extra information relating to the ice particle habit is the detailed scattering pattern rather than just using A_f. Also, the three central detector elements contain information that is not, so far, used.

5. SUMMARY AND CONCLUSIONS

The SID-2 probe is capable of counting, sizing and determining the phase of cloud particles. The laboratory derived sample volume (which determines the particle concentration) and size calibration have been validated against the FSSP and 2D-C probes in Stratocumulus, wave-cloud and Cirrus. SID-2 can discriminate between super-cooled drops and just-nucleation ice particles in mixed-phase cloud.

6. REFERENCES

Hirst E., Kaye P. H., Greenaway R. S., Field. P. and Johnson D. W., 2001: Discrimination of micrometre-sized ice and super-cooled droplets in mixed-phase cloud. *Atmos. Env.,* **35,** 33–47

Field P. R., Wood R., Brown P. R. A., Kaye P. H., Hirst E. and Greenaway R., 2003: Ice particle interarrival times Measured with a fast FSSP. *J. Atmos. Oceanic Tec.,* **20,** 249–261

APPENDIX

A. Laboratory calibrations

The size calibration of SID-2 was carried out in the laboratory using polystyrene latex spheres (PSL) spheres. For larger spheres the scattering cross-section is expected to scale with the projected area of the sphere. The detector response should therefore depend on the square of the particle size. The size calibration is also corrected for the different refractive index of 1.32 (water and ice average) and 1.6 (polystyrene). For spherical particles, the diameter is

$$D = 2.2\overline{S}^{0.5} \tag{1}$$

where $\overline{S}$ is the mean outer detector response. The angular dependence of scattering from ice crystals is expected to be different from spheres. For scattering angles corresponding to the outer detector ring, the ice crystals are undersized by a factor 1.7, ignoring crystal habit details.

The particle number concentration (cm^{-3}) is given by $\frac{f}{AV}$, where f is the count frequency (s^{-1}), A is the area of the triggering zone and V is the average particle velocity (which is equated to the true airspeed in-flight). The trigger is defined by the scattering from an area within the laser beam into two photomultiplier tubes. The trigger area depends on the particle size and phase (laboratory tests indicate $A = 0.88$mm^2 for 25μm ice particles.

B. Data processing

Each detector element has a different gain. The non-uniformity of the detector element response is corrected for by taking a large number of particles and assuming that on average the particle orientation is random. (The gain ranges from 0.58 to 1.88, where 1.0 is the average response).

Each detector element also has a different background noise level. This is temperature dependent and therefore varies during the flight. To determine the noise levels, all detector elements are read every second without the need for a trigger. The background levels are derived from these 'forced-particles' when in clear air.

For each triggered particle, the variation of the scattered light intensity around the azimuthal detector elements is calculated. This asphericity is given by,

$$A_f = \frac{k\sqrt{\sum_{i=1}^{n}\left(\overline{S} - S_i\right)^2}}{\overline{S}} \tag{2}$$

where S_i is the i'th detector element response out of n elements, and k is a scale factor so that $A_f < 100.0$.

The SID-2 data acquisition counts particles that are triggered but not read-out due to electronics dead time. These 'missing particles' are included in the time-series by distributing randomly over the relevant size-spectrum.

C. Flight details

D. Scattering patterns

The scattered light intensity onto each outer detector element for a sample of particles from each of the flight runs are shown in figs. 7–10. For all detector elements the response $2.2S_i^{0.5}$ is given as polar plots. Hence plot area is proportional to particle cross-section area, and for spherical particles (with uniform azimuthal response) plot radius is proportional to particle radius. Each figure uses the same size scale.

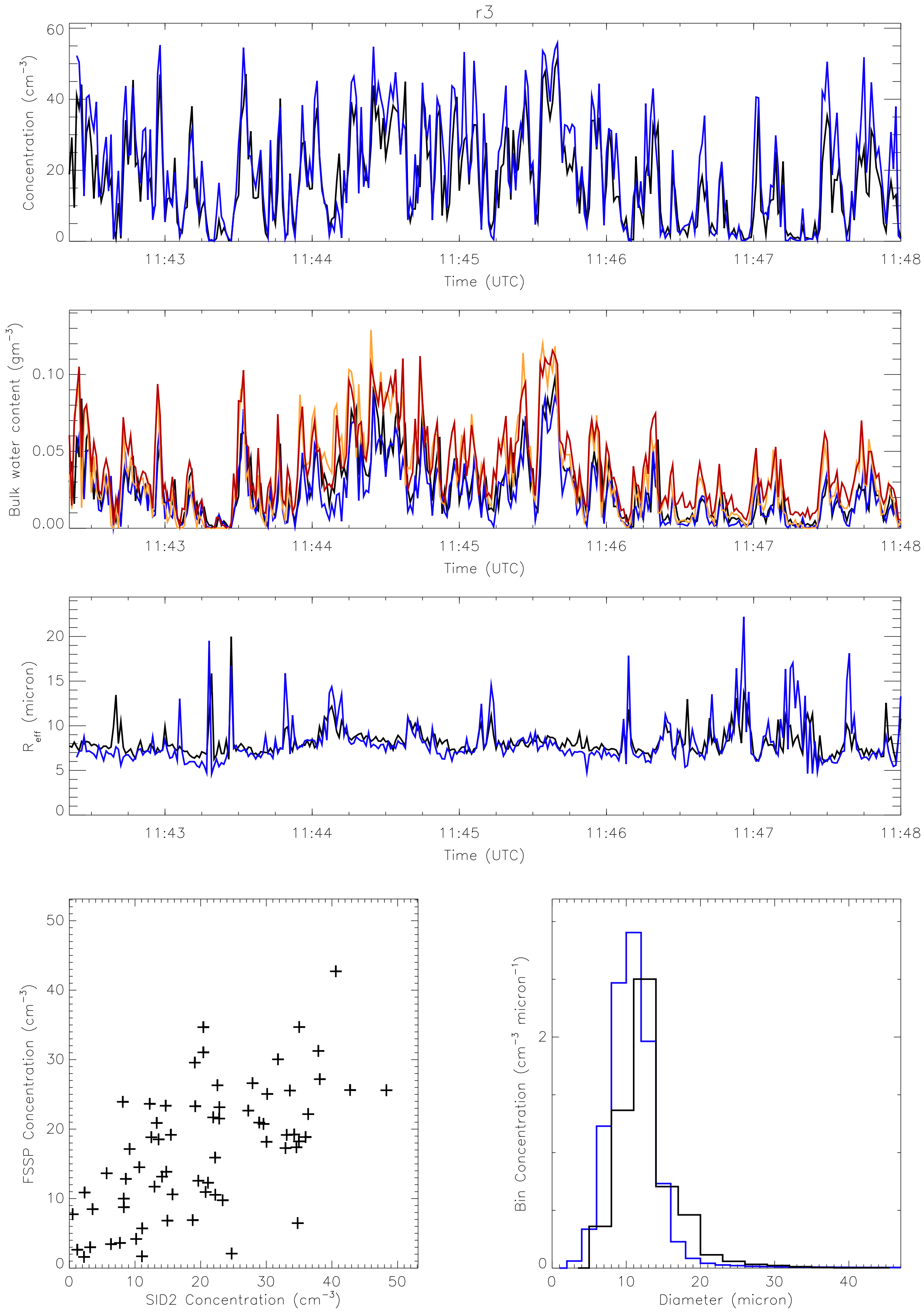

Figure 1: The blue line is SID-2, black is FSSP, red is Johnson-Williams LWC and orange is Nevzorov LWC. The time-series are 1 second data, the scatter-plot is averaged over 5 second intervals.

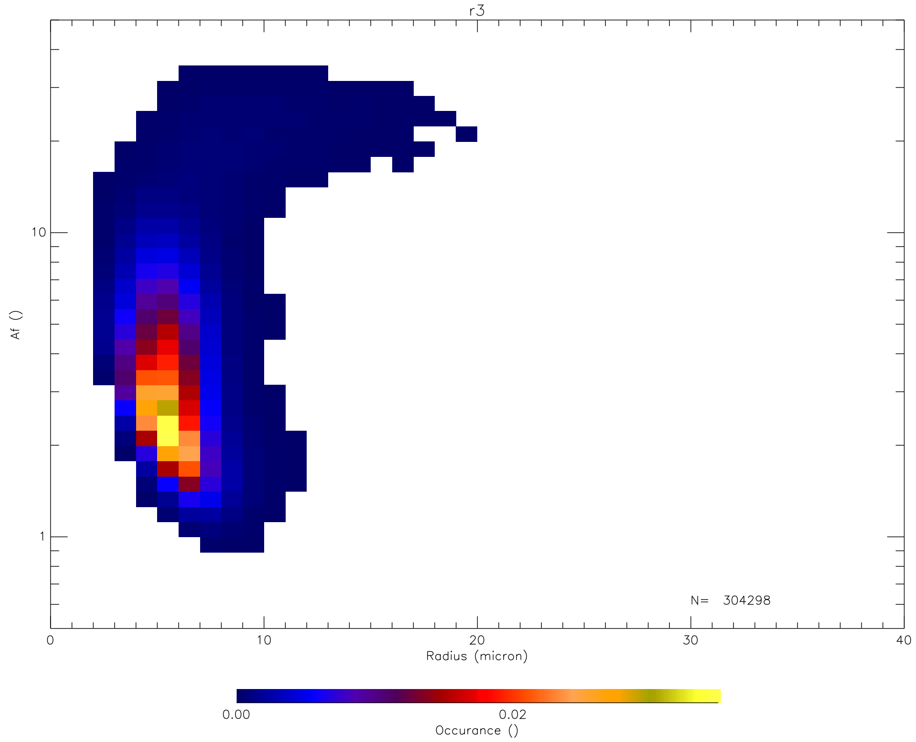

Figure 2: Stratocumulus cloud drops.

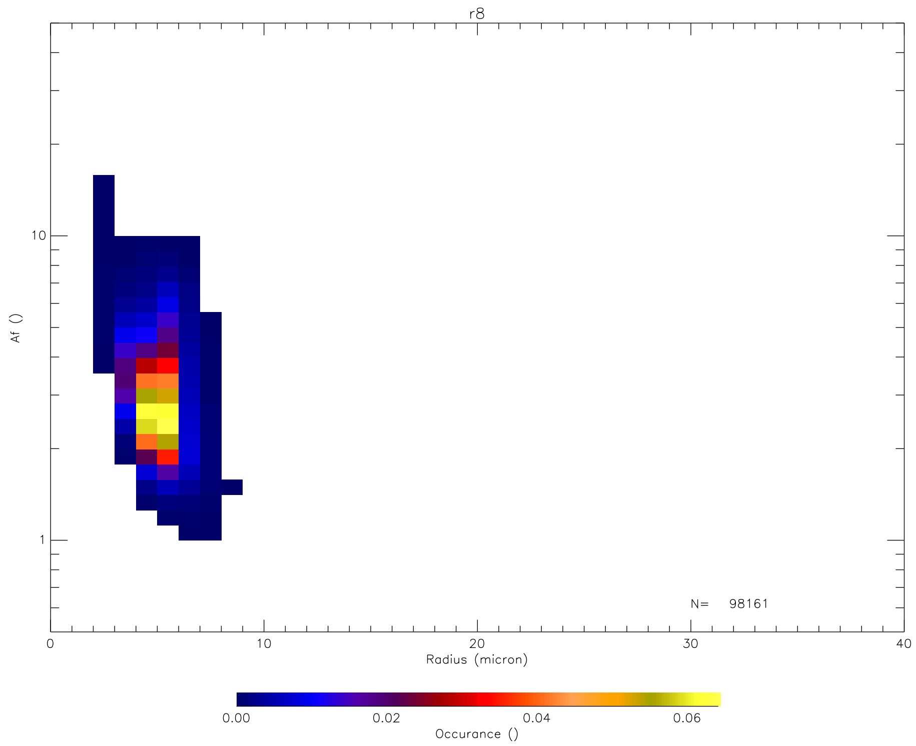

Figure 3: Wave-cloud super-cooled drops.

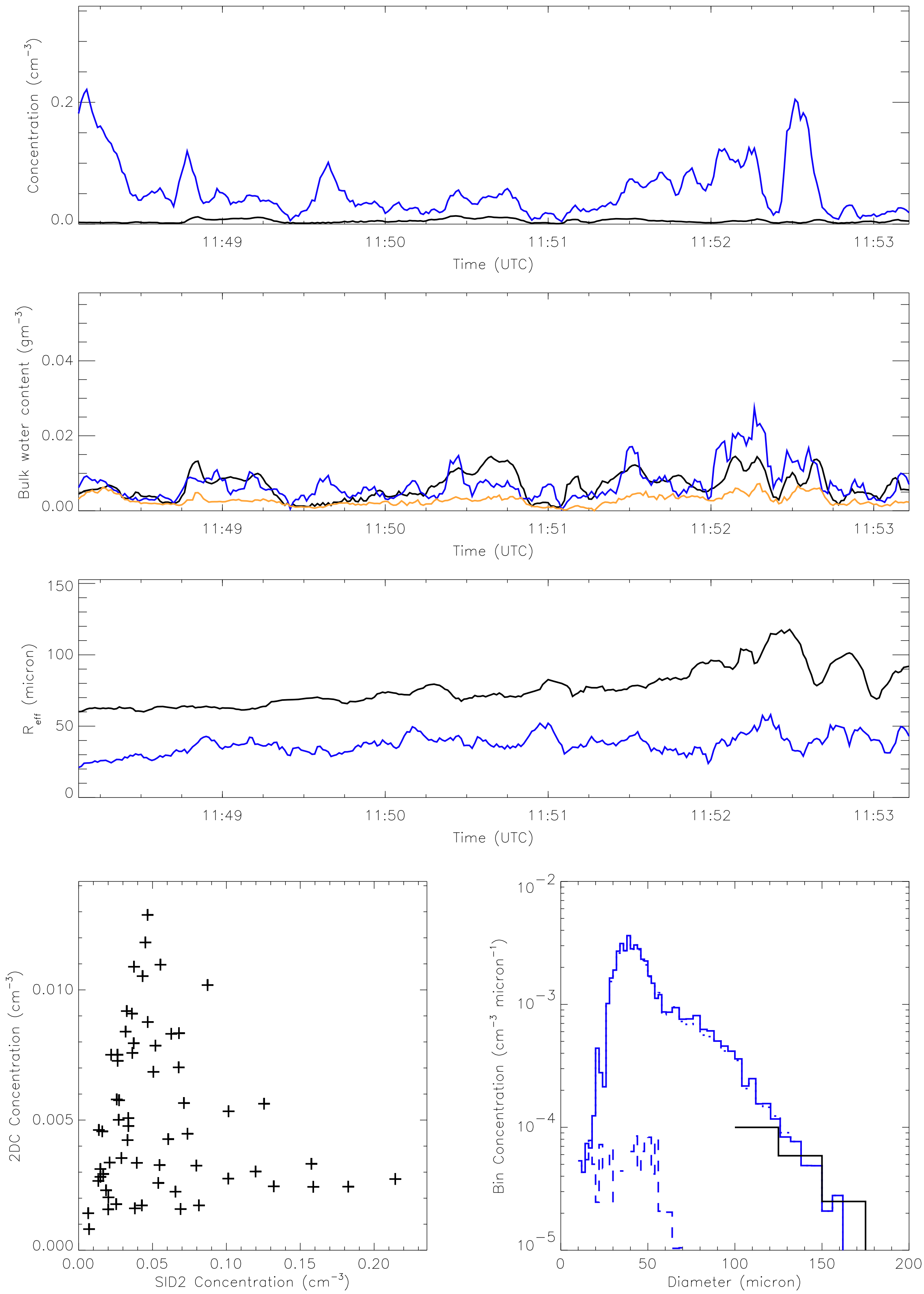

Figure 4: The blue line is SID-2, black is 2D-C, orange is Nevzorov TWC.

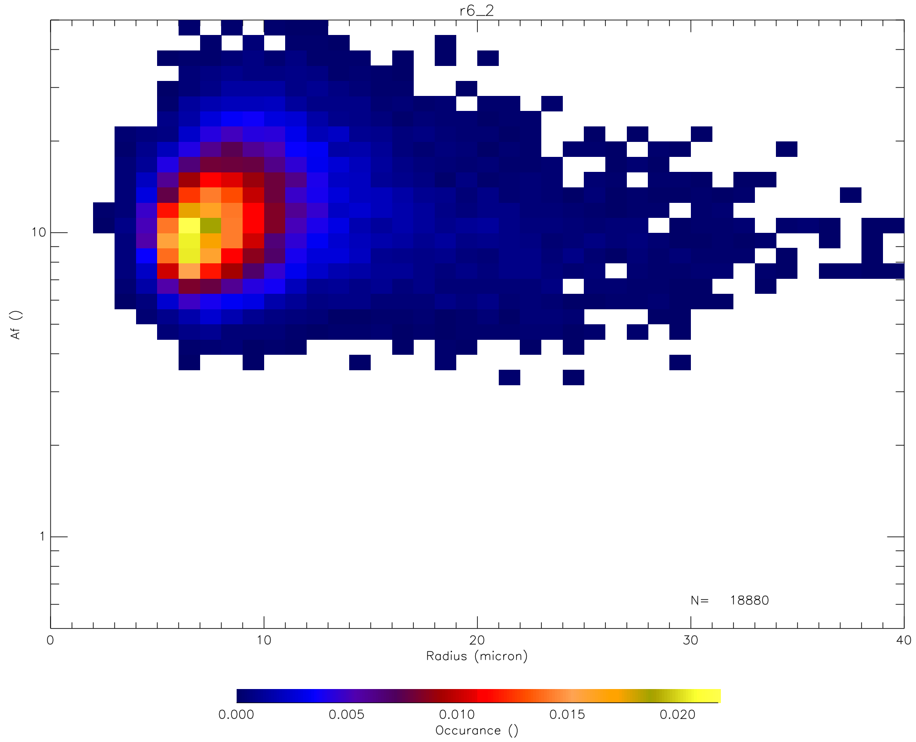

Figure 5: Cirrus pristine ice particles.

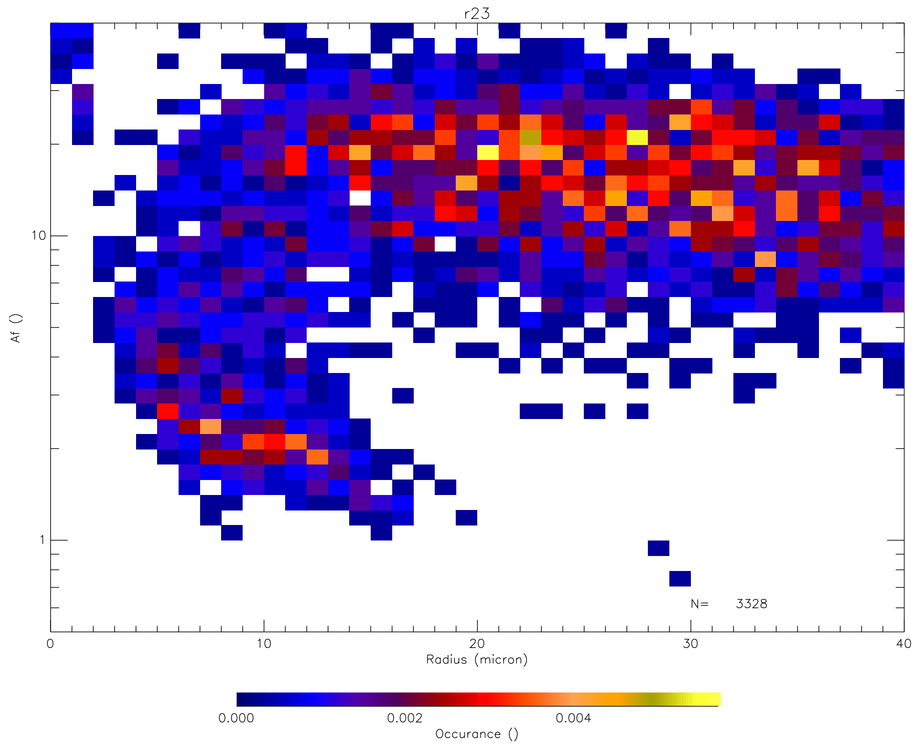

Figure 6: Cumulus mixed-phase.

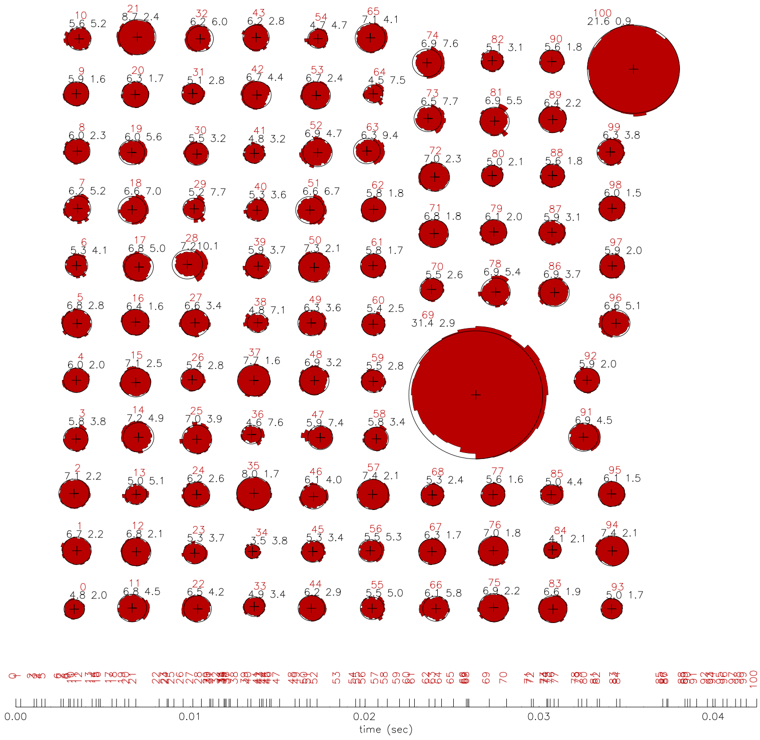

Figure 7: Stratocumulus cloud drops. The red particle number indicates the order of arrival. The two black numbers are the particle radius and A_f value. The black circle represents the calculated particle radius.

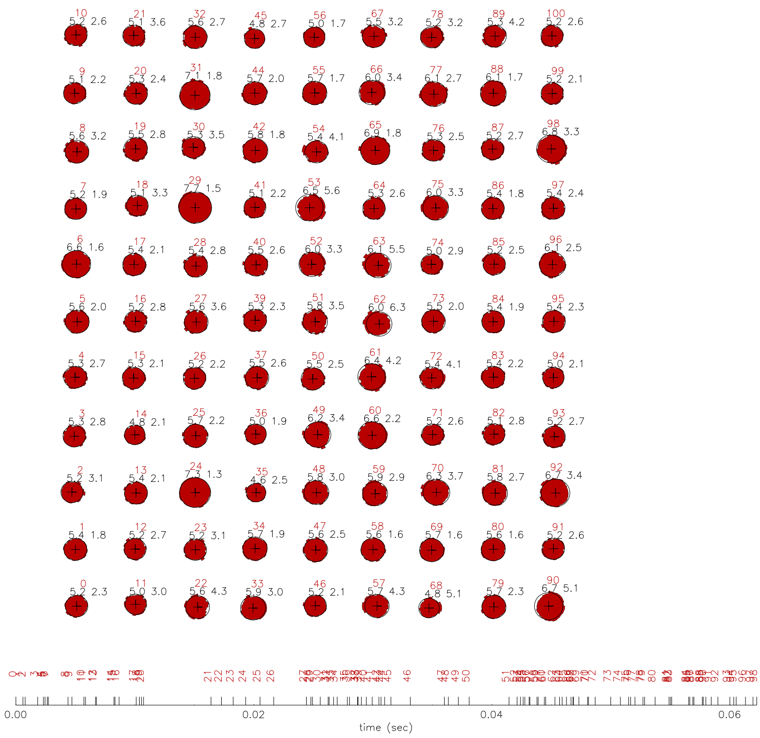

Figure 8: Wave-cloud supercooled drops.

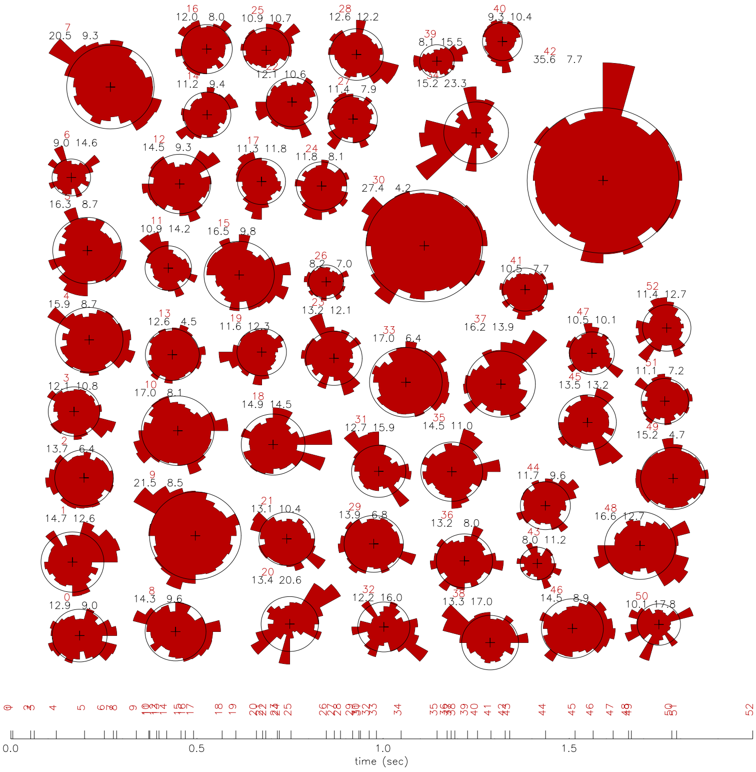

Figure 9: Cirrus pristine ice particles.

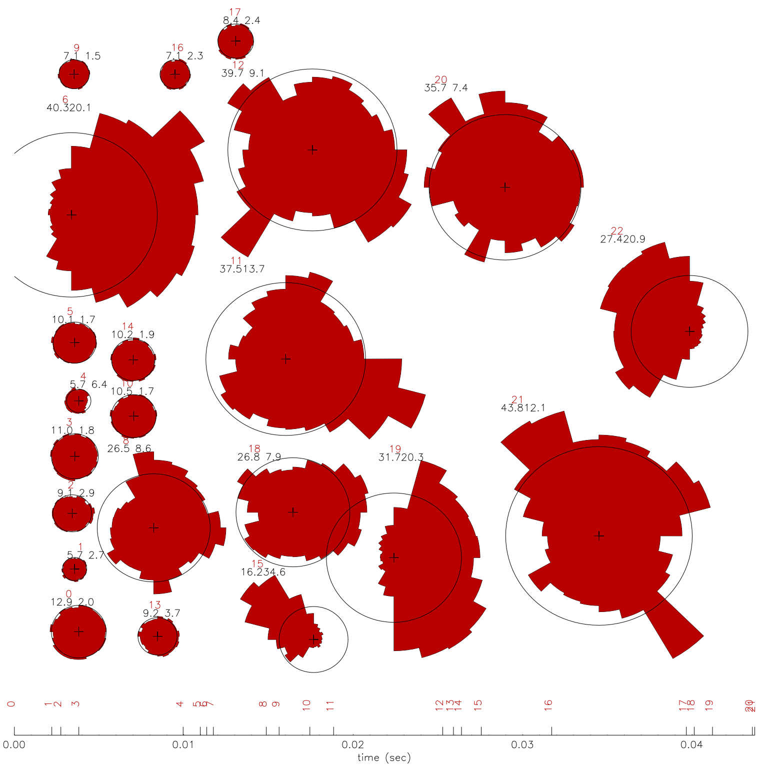

Figure 10: Cumulus mixed-phase.